IUST
Iran University of Science and Technology

Iranian Journal of Electrical and Electronic Engineering

Journal Homepage: ijeee.iust.ac.ir

Research Paper

Segmented Hybrid-PM Machines for Electric Vehicles; Semi-Analytical, Numerical and Experimental Study

A. Jabbari*(C.A.), and A. Baderan*

Abstract: In new generations of wind turbines and electric vehicles, cost reduction, efficiency improvement, enhanced reliability, extended maintenance life, noise and vibration reduction, as well as environmental considerations, are of great importance. In the meantime, segmented hybrid-permanent magnet (SHPM) machines, mainly the technology that combines segmented-PMs with different materials, dimensions and magnetization orientation, provide an opportunity to satisfy these demands. In this research, while presenting nine topologies of SHPM generator with segmented-PM rotor based on the Taguchi design of experiments method, a simple precise semi-analytical model is offered based on the subdomain method to estimate the magnetic performance characteristics of the SHPM machine. Magnetic partial differential equations (MPDEs) have been expressed in a pseudo-Cartesian coordinate system, and by using the suitable boundary conditions (BCs) and interface conditions (ICs), the general solution and their Fourier coefficients have been extracted using the separation of the variables approach. The performance characteristics of nine investigated SHPM machines were compared semi-analytically and numerically. A prototype SHPM machine has been fabricated and the results of semi-analytical modeling have been compared with the results of finite element analysis (FEA) method and the experimental tests in generating (charging mode). The FEA simulation and experimental test results have a maximum error percentage of about 3, confirming the high accuracy of the provided semi-analytical model. A comparison of induced voltage, torque ripple and magnetic torque is done between the studied topologies.

Keywords: Segmented Hybrid-PM Machine, Semi-Analytical Modeling, Design Concept, FEA, Experimental Test.

Nomenclature

Parameter	Description
T_e	Electromagnetic torque
L_s	Axial length of the motor
R_e	Effective radius
N_c	Number of conductors per slot
C	A matrix connection between the stator slots and phase connections
φ	The slot flux
k_f	The stator fill factor
S	The area of the stator slot
ω	The rotor angular speed
ψ_a	flux linkage per phase A
I_A	The peak current in phase A
E_a	The phase A back-emf
L_a	Self- inductance of phase A
M_{AB}	mutual inductance of phase A and phase B
N	the number of phase turns
φ_{AB}	magnetic flux in phase A and B
I_B	the peak current in phase B

Iranian Journal of Electrical & Electronic Engineering, 2023. First received 01 Feb 2023 and accepted 23 Oct 2023.
* The authors are with the Department of Mechanical Engineering, Faculty of Engineering, Arak University, Arak, Iran.
E-mails: a-jabbari@araku.ac.ir, shakeri@nit.ac.ir.
Corresponding Author: A. Jabbari.
https://doi.org/10.22068/IJEEE.19.3.2792

1 Introduction

OVER the past decade, multiple PM machine topologies have emerged as one of the hottest research topics in the electromechanical field. Rare earth PM machines exhibit higher torque and efficiency compared to conventional PM machines and are currently used in various torque speed level systems [1-2]. High-torque, low-speed applications such as Wind turbines and electric vehicles typically combine high-speed electric machines with mechanical drive trains [3]. These expensive systems can inherently suffer from high levels of acoustic noise, mechanical vibration, and maintenance issues. However, rare earth PM machines are expensive compared to their traditional counterparts. Electromagnetic torque ripple, reluctance torque ripple, and cogging torque are the three main components of system noise, vibration, and pulsating torque phenomena that can lead to desired performance. SHPM machines, especially techniques that combine segmented PM with different materials, different dimensions, and different magnetization directions, offer a way to meet these needs. In other words, in SHPM machines, the PM rotor consists of an optimal cost-effective PM combination that largely eliminates system problems in addition to meeting performance requirements.

There are many reports on the use of PM machines in the field of electric vehicles. In the work [4], a low rare earth interior permanent magnet synchronous machine (LRE-IPMSM) was investigated. They applied a multi-objective optimization technique to explore the effects of PM thickness and width on machine performance and optimized the PM width. In the work [5], an optimization study is performed to minimize the torque ripple component of a 150 kW interior PM synchronous machine with delta configuration rotor magnets used in electric vehicles. They combined analytical calculations with finite element analysis and also used genetic algorithm methods. The effect of rotor configuration on the performance of internal permanent magnet (IPM) electric machines has been studied in [6]. They compared different machine topologies with the same amount of PM in terms of torque capability, flux-weakening capability, and demagnetization. A rare-earth free PM traction machine has been developed for C-segment electric vehicles [7]. Four different ferrite PM synchronous machine topologies with different magnet arrangements and number of magnetic pole pairs were presented, selected for their high probability, and compared using a computer FEA tool. In the work [8], a new brushless machine with PM flux mnemonics is proposed and implemented as an integrated starter generator for electric vehicles. The key lies in the integration of the memory engine concept, the flux mnemonic, and the double protrusion PM machine. Therefore, it offers the advantages of mechanical robustness, controllable air-gap flux, and efficient on-line PM magnetization. By further using outer rotor and double layer stator topology, the proposed ISG achieves direct drive capability and low armature reaction. In the work [9], researchers discussed the analysis of new PM machine topologies. It also compares different types of electric motors suitable for automotive applications in terms of their strengths and weaknesses. In the work [10], authors present an automated methodology aimed at minimizing the PMSM design time for HEV applications through a systematic approach and parallel computation.

Applications of SHPM machines in electric vehicles have been investigated in several papers. In the work [11], the researcher proposed the two-layer HPM and the non-uniform air-gap motor topology for the EV applications. Simulation results indicate that the proposed motor has a favorable flux-weakening ability and a wide speed range. Design and research of 6-phase in-wheel surface-mounted permanent magnet motors (SPMs) and internal permanent synchronous motors for electric vehicle (EV) applications [12].
Several methods have been proposed to reduce torque ripple in PM machines. Some known techniques include optimal pole/stator slot skew angles [13-16], optimal pole width to pole pitch ratio or slot width to slot pitch ratio [17], dummy slots [18-21], and magnet segmentation [22]. The most common method used to reduce the pulsating torque component of PM machines is magnet segmentation. This method offers the possibility of combining magnet segments with different materials, different sizes, and magnetization directions. Determining the exact number and dimensions of the segments is very important when applying the magnet segmentation method. Accurate estimation of the magnetic vector potential is therefore essential to calculate mechanical performance such as cogging torque, electromagnetic torque, back electromotive force, self-inductance and mutual inductance, and to determine the optimum values of design parameters. Various methods, including semi-analytical and numerical methods, have been used to estimate magnetic flux density distributions in electrical machines. Accurate results can be obtained using numerical techniques such as FEA, but these techniques are very time consuming, especially in the early stages of engineering design.

Powerful commercial software is currently used to design PM machines. Numerical techniques, such as FEM approaches, are often used in this program to calculate the magnetic properties of machine performance. For some of them, it is easy to

parametrically model conventional electrical machines and find their magnetic performance. However, research shows that parametric modeling of geometry and parametric mapping of electrical and magnetic properties of SHPM machines are not considered in existing commercial software. Therefore, modeling them numerically is very difficult and time consuming. Analyses suitable for modeling electrical machines, such as conformal maps [23-25], and subdomain methods [27-43], which take into account the relative permeability of slots, have been published for initial design steps and design optimization.

An accurate solution for enabling parametric modeling of arbitrary topologies of SHPM machines and estimating the magnetic performance of SHPM machines quickly and accurately is analytical modeling based on the subdomain approach. In this method, the SHPM machine is divided into several different regions and the partial differential equations (PDEs) are rewritten for each region. The general solution of the PDE is computed by the separation of variables method with the corresponding boundary conditions (BC), then the initial conditions (IC) of the adjacent region are used to compute the Fourier coefficients of these PDEs.

A comprehensive review of recent research confirms that many researchers have analytically modeled PM machines. In the general classification of PM machine modeling, these models consider magnetization orientation (radial [50], parallel or Halbach, [51]), PM placement (surface mount, surface inset, or spoke type [44], [45, 53]), whether it occurs with infinite permeability [54] or finite permeability, and the use of linear or nonlinear ferromagnetic materials [55-59]. A simple modeling of a segmented PM machine is presented in [22, 60]. Therefore, there are no reports of semi-analytical models of SHPM machines. However, some performance data for SHPM machines has been presented separately in other studies and can be used to develop semi-analytical models for SHPM machines.

In this research study, a new SHPM machine is first presented and then a semi-analytical model is refined to accurately calculate the features of the machine. The five different topologies of presented SHPM machines are considered and the features of these machines are compared. Within the model developed, the effects of stator slots, placement, and magnetic orientation of the PM can be considered. To obtain the accuracy of the improved model, the SHPM machine with specific geometric size and electromagnetic parameters was considered. The performance of the SHPM machine is first estimated by a semi-analytical model and then compared with results calculated by numerical methods using FEA-based software. To evaluate the accuracy of the developed model, a prototype of the SHPM machine is built and semi-analytical and experimental waveforms are extracted. These comparisons confirmed a maximum error of approximately 3% for the semi-analytical, FEA, and experimental results, indicating that the improved model has a high level of accuracy. The proposed SHPM machine employs a segmented pole rotor design to reduce machine cost, reduce ripple torque, reduce demagnetization limitation, and increase machine dynamic strength. Using cost-effective SHPM technology reduces the risk of demagnetization, thermal issues, and system weight.

This paper is organized as follows: Section 2 describes the design concept, working principle of the proposed SHPM machine, and the development of the magnetic semi-analytical model. Section 3 covers FEM simulation of the machine is performed in commercial software. A prototype SHPM machine has also been manufactured and experimental tests are presented in Section 4. This section compares results from semi-analytical models, FEA simulations, and experimental tests.

2 Development of Electromagnetic Semi-Analytical Model

In this section, we introduce the concept of the proposed electric SHPM machine and express the presented semi-analytical method to estimate the features of the SHPM machine.

2.1 SHPM Machine Topology

Figure 1 shows schematics of five topologies of electric PM machines. In the rotor section, the permanent magnet arrangements are as shown in Figure 1: conventional surface-mounted PMs, surface-inset PMs, consequent-pole PMs, magnets segmented with similar PM materials, and heterogeneous (hybrid) magnets segmented in PM materials (a), (b), (c), (d) and (e) respectively. The last two topologies can have similar/dissimilar PMs with similar/dissimilar magnetization directions. The stator slots are also equipped with several coils in a three-phase winding arrangement.

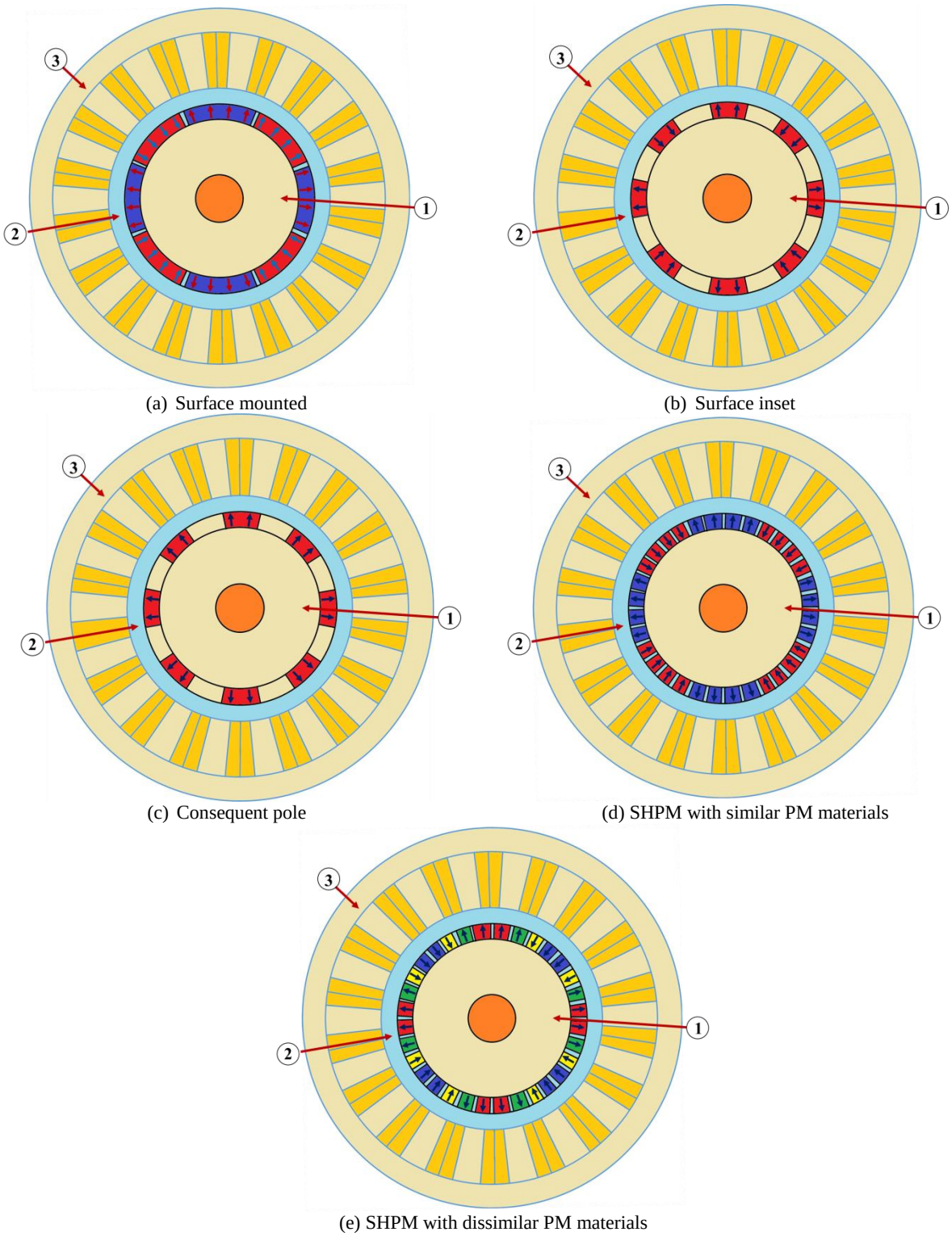

(a) Surface mounted (b) Surface inset

(c) Consequent pole (d) SHPM with similar PM materials

(e) SHPM with dissimilar PM materials

Fig. 1 Schematics representation of five topologies of the PM electric machine. 1- rotor, 2-airgap, 3-stator.

2.2 Electromagnetic/Magnetic Modeling

In this section, we present a semi-analytical method of the magnetic features of the investigated SHPM machine. Figures 2(a) and (b) show the 2D geometrical features of the SHPM machine in polar and pseudo-Cartesian coordinates, respectively. As you can see, the machine is divided into the 10

subdomains. These regions are represented by 1-10 labels in the 2D shape model of the machine. Field patterns can be repeated in each sub-area of the machine. These areas are then denoted by the i, j, k, and l indices. For example, the magnetic poles of a surface-mount segmented permanent magnet rotor are denoted by 1(i), where 1 is the area number and i is the number of poles from 1 to 6.

2.2.1 Electromagnetic/Magnetic Modeling

To estimate the performance characteristics of the SHPM machine, partial differential equations (Laplace's equation for the periodic air gap and Poisson's equation for the aperiodic PM and windings) are used with a variable separation approach that considers solving the appropriate variables. BC, find the magnetic vector potential waveform for each region. The IC between two or more adjacent regions can then be used to determine the Fourier coefficients of the equation. The magnetic vector potential can be used to compute the radial and tangential components of the magnetic flux density. Maxwell's equations are used to estimate the electromagnetic torque.

In general, Laplace's equation and Poisson's equation in the polar coordinate system of a rotating electrical machine are represented by Equations (1) and (2).

$$\frac{\partial^2 A(r.\theta)}{\partial r^2} + \frac{1}{r}\frac{\partial A(r.\theta)}{\partial r} + \frac{1}{r^2}\frac{\partial^2 A(r.\theta)}{\partial \theta^2} = 0 \quad \text{for} \begin{cases} R_1 \le r \le R_2 \\ \theta_1 \le \theta \le \theta_2 \end{cases} \tag{1}$$

$$\frac{\partial^2 A(r.\theta)}{\partial r^2} + \frac{1}{r}\frac{\partial A(r.\theta)}{\partial r} + \frac{1}{r^2}\frac{\partial^2 A(r.\theta)}{\partial \theta^2} = f(r.\theta) \quad \text{for} \begin{cases} R_1 \le r \le R_2 \\ \theta_1 \le \theta \le \theta_2 \end{cases} \tag{2}$$

By rewriting the partial differential equations in the pseudo-Cartesian coordinate system [59], we can obtain a simpler mathematical model in hyperbolic form for rotating electrical machines. Figure 2 shows the geometry of the 2D machine model studied in the coordinate system proposed by Jabbari. The Laplace and Poisson equations in the pseudo-Cartesian coordinate system are given by (3) and (4), respectively.

$$\frac{\partial^2 A}{\partial t^2} + \frac{\partial^2 A}{\partial \theta^2} = 0 \quad \text{for} \begin{cases} t_1 \le t \le t_2 \\ \theta_1 \le \theta \le \theta_2 \end{cases} \tag{3}$$

$$\frac{\partial^2 A}{\partial t^2} + \frac{\partial^2 A}{\partial \theta^2} = f(t.\theta) \quad \text{for} \begin{cases} t_1 \le t \le t_2 \\ \theta_1 \le \theta \le \theta_2 \end{cases} \tag{4}$$

where $t = ln(\frac{r}{R_1})$, $t_1 = ln\left(\frac{R_2}{R_1}\right)$ and $t_2 = 0$.

The PDE equations related to each subdomain are presented in Table 1.

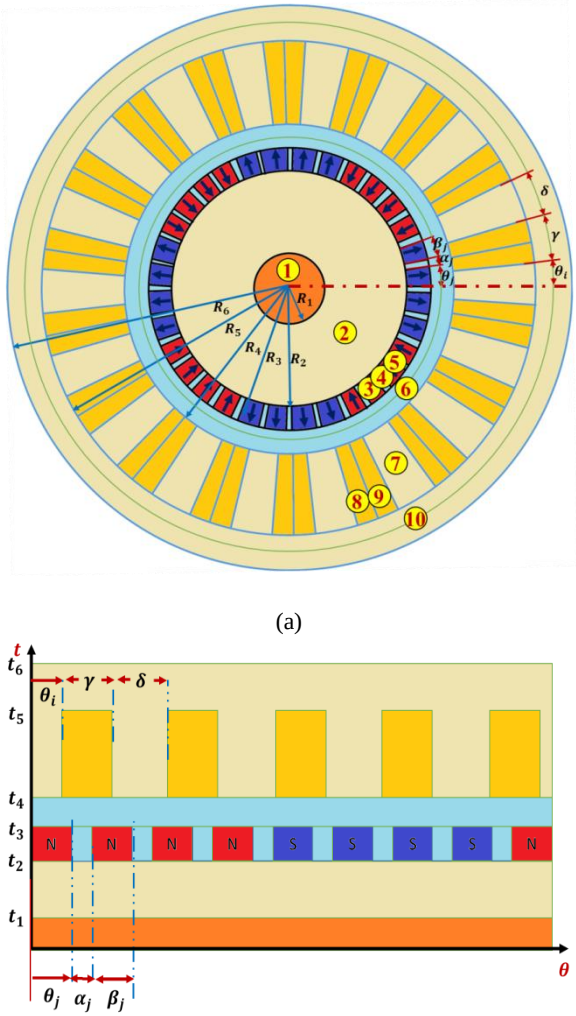

(a)

(b)

Fig. 2 Definition of the SHPM machine subdomains in the (a) $R-\theta$ coordinates system, (b) $t-\theta$ coordinates system.

Figure 3 shows the PDE, BC, and IC corresponding to each region of the investigated SHPM machine. These equations are presented in the quasi-Cartesian coordinate system and are shown for the domains

corresponding to each region in Table 1. The BCs for various areas of the system are shown in Table 2 for t-edges and θ-edges.

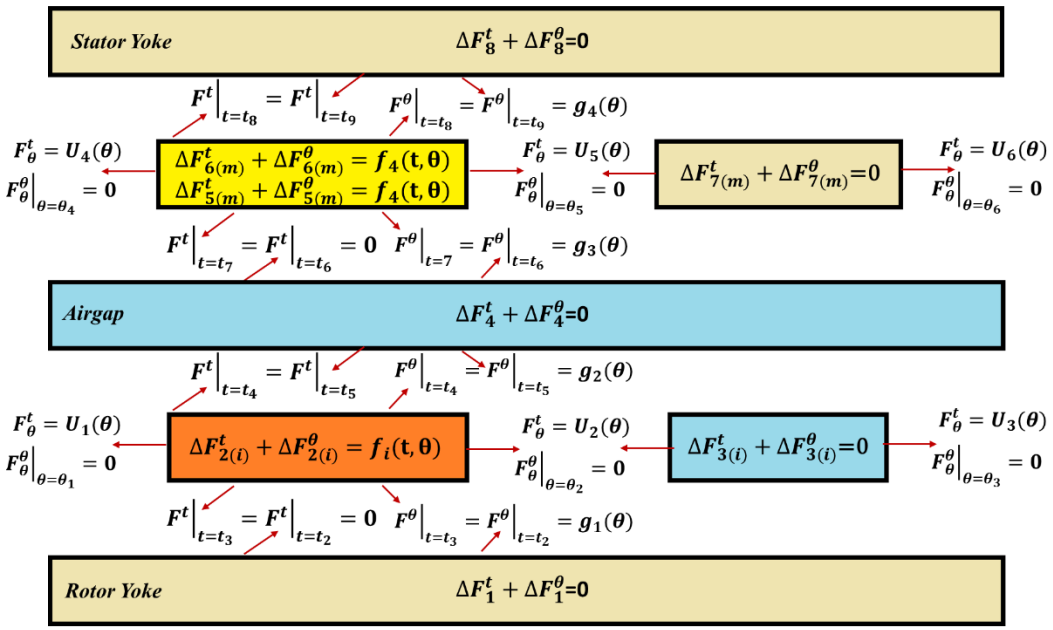

Fig. 3 The corresponding PDEs, BCs and ICs of each subdomain.

Table 1 PDE equations related to each subdomain.

PDEs equations		Region Ω	Domain
$\frac{\partial^2 A_\Omega}{\partial t^2} + \frac{\partial^2 A_\Omega}{\partial \theta^2} = 0$	(Laplace's Equation)	I (air-gap)	$\begin{cases} t_3 = ln(R_3/R_4) \le t \le t_4 = 0 \\ 0 \le \theta \le 2\pi \end{cases}$
$\frac{\partial^2 A_\Omega}{\partial t^2} + \frac{\partial^2 A_\Omega}{\partial \theta^2} = -\mu_0 J$	(Poisson's Equation)	j (stator slot)	$\begin{cases} t_4 = ln(R_4/R_5) \le t \le t_5 = 0 \\ \theta_i \le \theta \le \theta_i + \gamma \end{cases}$
$\frac{\partial^2 A_\Omega}{\partial t^2} + \frac{\partial^2 A_\Omega}{\partial \theta^2} = -\frac{\mu_0}{r}(M_\theta - \frac{\partial M_r}{\partial \theta})$	(Poisson's Equation)	I (PM rotor)	$\begin{cases} t_2 = ln(R_2/R_3) \le t \le t_3 = 0 \\ \theta_j \le \theta \le \theta_j + \alpha \end{cases}$
for radial magnetization $\begin{cases} M_{rn} = \frac{4B_r}{\mu_0 n\pi}.Sin(\frac{n\pi\alpha_p}{2}) \\ M_{\theta n} = 0 \end{cases}$			
for parallel magnetization $\begin{cases} M_{rn} = \frac{B_r}{\mu_0}\alpha_p.[A_{1n}(\alpha_p) + A_{2n}(\alpha_p)] \\ M_{\theta n} = \frac{B_r}{\mu_0}\alpha_p.[A_{1n}(\alpha_p) - A_{2n}(\alpha_p)] \end{cases}$	$A_{1n}(\alpha_p) = Sin((np+1)\frac{\pi\alpha_p}{2p})/(np+1)\frac{\pi\alpha_p}{2p}$ $A_{2n}(\alpha_p) = \begin{cases} Sin((np-1)\frac{\pi\alpha_p}{2p})/(np-1)\frac{\pi\alpha_p}{2p} & for\ \ np \ne 1 \\ 1 & for\ \ np = 1 \end{cases}$		

Table 2 θ-edges interface conditions (ICs)

$\boldsymbol{r = R_2}$		$\boldsymbol{r = R_3}$	
$A_{z1(i)}\big\|_{t=t_2} = A_{z2}\big\|_{t=t_3}$	$\forall\theta \in [\theta_1.\theta_2]$	$A_{z3(j)}\big\|_{t=t_5} = A_{z2}\big\|_{t=t_4}$	$\forall\theta \in [\theta_3.\theta_4]$
$D_{z1(i)}\big\|_{t=t_2} = D_{z2}\big\|_{t=t_3}$	$\forall\theta \in [\theta_1.\theta_2]$	$D_{\theta3(j)}\big\|_{t=t_5} = D_{\theta2}\big\|_{t=t_4}$	$\forall\theta \in [\theta_3.\theta_4]$
$\boldsymbol{r = R_4}$		$\boldsymbol{r = R_5}$	
$F_{z5(k)}\big\|_{t=t_7} = F_{z4}\big\|_{t=t_6}$	$\forall\theta \in [\theta_5.\theta_6]$	$A_{z7(k)}\big\|_{t=t_9} = A_{z5(k)}\big\|_{t=t_8}$	$\forall\theta \in [\theta_7.\theta_8]$
$D_{\theta5(k)}\big\|_{t=t_7} = D_{\theta4}\big\|_{t=t_6}$	$\forall\theta \in [\theta_7.\theta_8]$	$D_{\theta7(k)}\big\|_{t=t_9} = D_{\theta5(k)}\big\|_{t=t_8}$	$\forall\theta \in [\theta_7.\theta_8]$

The general solutions of the partial differential equations in the periodic and aperiodic domains considering the given BC are given in Table 3. Separation of variables is used to estimate the magnetic vector potential of each region. IC is applied to find the Fourier coefficients of the equation.

Table 3 The general solution of Laplace's and Poisson's equations for the proposed SHPM machine.

Region Ω	General solution
j, i	$A_\Omega(t.\theta) = {a_0}^\Omega + {b_0}^\Omega t + f(t) + \sum_{h=1}^{\infty}\left(\begin{array}{c} {a_h}^\Omega \frac{\varphi}{h\pi}\frac{F(\frac{h\pi}{\varphi}(t-t_i))}{G(\frac{h\pi}{\varphi}(t_j-t_i))} \\ +{b_h}^\Omega \frac{\varphi}{h\pi}\frac{F(\frac{h\pi}{\varphi}(t-t_i))}{G(\frac{h\pi}{\varphi}(t_j-t_i))}\end{array}\right) Cos\left(\frac{h\pi}{\varphi}(\theta-\emptyset)\right)$
I	$A_\Omega(\mathrm{t}.\theta) = \sum_{n=1}^{\infty}\left(\begin{array}{c}\frac{1}{n}\frac{F\left(n(\mathrm{t}-\mathrm{t_i})\right)}{G\left(n(\mathrm{t_j}-\mathrm{t_i})\right)}{a_n}^\Omega \\ +\frac{1}{n}\frac{F\left(n(\mathrm{t}-\mathrm{t_j})\right)}{G\left(n(\mathrm{t_i}-\mathrm{t_j})\right)}{b_n}^\Omega + g(t)\end{array}\right) Cos(n\theta) + \sum_{n=1}^{\infty}\left(\begin{array}{c}\frac{1}{n}\frac{F\left(n(\mathrm{t}-\mathrm{t_i})\right)}{G\left(n(\mathrm{t_j}-\mathrm{t_i})\right)}{c_n}^\Omega \\ +\frac{1}{n}\frac{F\left(n(\mathrm{t}-\mathrm{t_j})\right)}{G\left(n(\mathrm{t_i}-\mathrm{t_j})\right)}{d_n}^\Omega + g(t)\end{array}\right) Sin(n\theta)$

Where $f(t) = -\frac{1}{2}\mu_0 J_i\left(e^{-t_4}t + \frac{1}{2}e^{-2t+t_4}\right)$, $\varphi = \gamma$, $\emptyset = \theta_i$, ${b_0}^\Omega = {b_h}^\Omega = 0$, $t_i = t_4$ and $t_j = t_5$, $F = Cosh$, G=$Sinh$ at i region, $F = Cosh$, $G = Sinh$, $t_i = t_3$, $t_j = t_2$, $f(t) = X_n(t)Cos\left(\frac{n\pi\alpha_p}{2\alpha_r}\right)$.

$$X_n(t) = \left(1+\frac{1}{n}e^{(n+1)t}\right)f_n(t) - \frac{\mathrm{Cosh}(n(t-t_8))}{\mathrm{Cosh}(n(t_7-t_8))}\left(1+\frac{1}{n}e^{(n+1)t_7}\right)f_n(t_7)$$

$$f_n(t) = \begin{cases}\mu_0\dfrac{npM_{rn}+M_{\theta n}}{1-np^2}R_1e^{-t} & if\ np \neq 1 \\ -\mu_0\dfrac{M_{rn}+M_{\theta n}}{2}R_1e^{-t}ln(R_1e^{-t}) & if\ np = 1\end{cases}$$

3 Model and Machine Evaluation

In this section, we apply the implemented semi-analytical model to estimate the air-gap flux density waveform, magnetic torque, magnetic torque ripple, and induced voltage for the presented SHPM machine under generative mode of operation. Numerical simulations are performed in FEM software, and a prototype of the SHPM machine is also manufactured. The results of the semi-analytical method are validated by the results of FEM simulations and experimental tests. As shown in Table A1, the electromagnetic torque, flux linkage, back electromotive force, self-inductance, and mutual inductance can be calculated by A(1) through A(9) respectively.

3.1 Semi-Analytical Modeling and Taguchi Design of experiments Method

In this section, Taguchi's DOE method is used to study the effect of three parameters: the number of segments, the type of magnet, and the magnetization

direction of the magnet. The geometric and electromagnetic parameters of the investigated SHPM machine are given in Tables 4 and 5, respectively. These parameters and their assigned values are listed in the L9 array in Table 6.

Table 7 shows orthogonal arrays based on the Taguchi method, with nine tests proposed. A description of these combinations and the parameters for each experiment is shown in Table 8. Fig. 4 shows a schematic diagram of the rotor in each experimental test based on the Taguchi method.

Table 4 Geometrical parameters of the studied SHPM machine.

Symbol	Value	Symbol	Value
R_1	10	θ_j	72
R_2	28.5	α	32
R_3	33.5	β	28
R_4	34.5	δ	12
R_5	45.5	θ_i	24
R_6	57.5	γ	5
R: radius in mm, θ: mechanical degree			

Table 5 Magnetic and mechanical parameters of the studied SHPM machine.

Parameter/symbol		Unit	Value/Name
PM Type	NdFeB-N35	T	B_r =1.17
	Alnico-1		B_r =0.72
	SmCo-18		B_r =0.86
Lamination material		-	M19-0.5
Wire material		-	Cu
Number of conductors per slot		-	20
Rated speed (High speed rotor)		RPM	1500

Table 6 Design parameters and their levels.

Level / Parameter	L1	L2	L3
Segments No.	3	4	5
Material No.	1 (pure NdFeB)	2 (NdFeB+Alnico)	3 (NdFeB+SeCo+Alnico)
Magnetization Type	Radial	Tangential	Compound

Table 7 Orthogonal array table.

	1	2	3
1	1	1	1
2	1	2	2
3	1	3	3
4	2	1	2
5	2	2	3
6	2	3	1
7	3	1	3
8	3	2	1
9	3	3	2

Table 8 Design of Experiments based on the Taguchi approach.

Trial No.	Trial Combination	Description
1	1-1-1	3 segments of PMs, pure NdFeB with radial magnetization
2	1-2-2	3 segments of PMs, one NdFeB (in center) + two Alnico segments, all with tangential magnetization
3	1-3-3	3 segments of PMs, one NdFeB (in center with radial magnetization) + one Alnico+one SeCo segments, both with tangential magnetization
4	2-1-2	4 segments of PMs, pure NdFeB with tangential magnetization
5	2-2-3	4 segments of PMs, two NdFeB (in center with radial magnetization) + two Alnico both with tangential magnetization
6	2-3-1	4 segments of PMs, one NdFeB + one SeCO (in center) + two Alnico, all with radial magnetization
7	3-1-3	5 segments of PMs, all NdFeB, 3 segments in center with radial magnetization, two adjacent segments with tangential magnetization
8	3-2-1	5 segments of PMs, 3 NdFeB segments in center, two adjacent Alnico segments, all with radial magnetization
9	3-3-2	5 segments of PMs, one NdFeB segments in center, two adjacent SeCo and two Alnico segments, all with tangential magnetization

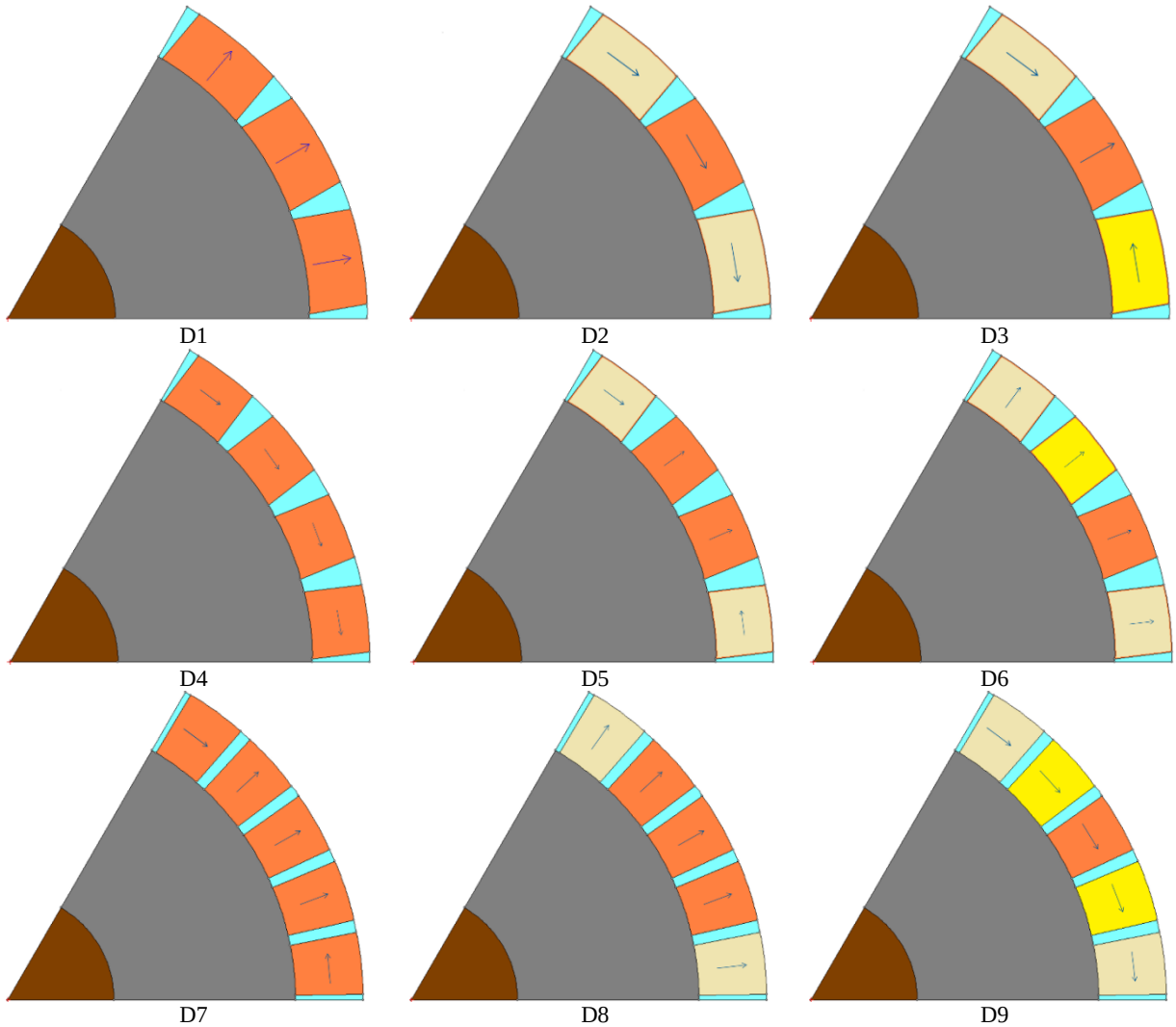

Fig. 4 Schematic representation of the proposed rotor combination based on L-9 array of the Taguchi method. NdFeB-35 ( ), Alnico-1 ( ), SeCo-18 ( ).

Analytically estimate the resulting electromagnetic torque and torque ripple values as shown in Table 9. Optimal conditions are shown in Table 10.

Figure 5 shows an analytical comparison of the electromagnetic torque waveforms of the initial (D1) and optimal (D10) designs. A comparison of the total cost of PM materials for each rotor investigated is calculated and compared in Table 11. It is evident that the optimum rotor torque ripple and magnet price are reduced by 75.28% and 36.9% respectively compared to the original design.

Table 9 Results analysis.

Trial No.	Average Electromagnetic Torque (N.m)	Torque Ripple (N.m)	Torque Ripple Percentage
1	15.749	0.9819	6.234
2	26.625	0.2566	0.963
3	48.470	0.4025	0.830
4	45.470	0.6195	1.362
5	25.867	0.3629	1.402
6	11.555	0.1699	1.47
7	35.186	0.5675	1.612
8	11.244	0.3255	2.894
9	32.633	0.2122	0.650

Table 10 Optimum condition and performance.

Column/Factor	Level Description	Level
1 (Seg. No)	5	3
2 (Material No.)	NdFeB + SmCo + Alnico	3
3 (Magnetization)	Tangential	2
Expected Result at Optimum Condition		12.624

Table 11 Total cost of permanent magnet materials for each studied machine.

Design type	PMs type/dimension (mm)	PM No.	Per PM price ($)		Total Price ($)	Price reduction (%)
D1 (Initial)	NdFeB/20*22*6	8	6.5	52	52	-
D2	3NdFeB/20*6*6	24	1.9	45.6	45.6	12.3
D3	1NdFeB/20*6*6	8	1.9	15.2	20.48	60.6
	2Alnico/20*6*6	16	0.33	5.28		
D4	1NdFeB/20*6*6	8	1.9	15.2	32.48	37.5
	1Alnico/20*6*6	8	0.33	5.28		
	1SeCo/20*6*6	8	1.5	12		
D5	4 NdFeB/20*5*6	32	1.7	54.4	54.4	-4.6
D6	2NdFeB/20*5*6	16	1.7	27.2	31.68	39.07
	2Alnico/20*5*6	16	0.28	4.48		
D7	1NdFeB/20*5*6	8	1.7	13.6	28.48	45.23
	2Alnico/20*5*6	16	0.28	4.48		
	1SeCo/20*5*6	8	1.3	10.4		
D8	5NdFeB/20*4*6	40	1.4	56	56	-7.6
D9	3NdFeB/20*4*6	24	1.4	33.6	37.6	27.69
	2Alnico/20*4*6	16	0.25	4		
D10 (Optimal)	1NdFeB/20*4*6	8	1.4	11.2	32.8	36.9
	2Alnico/20*4*6	16	0.25	4		
	2SeCo/20*4*6	16	1.1	17.6		

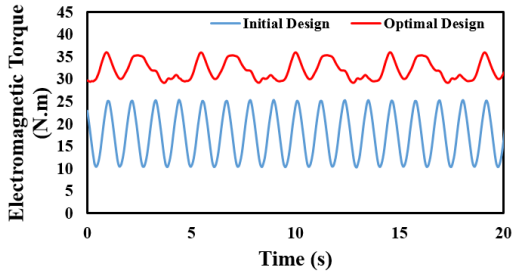

Fig. 5 Analytical estimation of electromagnetic torque waveforms for initial and optimal designs.

3.2 Semi-Analytical and FEA Result Comparison

The performance of the proposed machine in production (load) mode is estimated semi-analytically and numerically. We apply 2-D FEA to calculate the magnetic vector potential and magnetic field distribution in the air gap region, as shown in Figs. 6 and 7, respectively. Numerical and semi-analytical comparisons of magnetic flux density waveforms in the air gap region of the investigated machine are shown in Figs. 8, 9, and 10. The performance of the presented SHPM machine is investigated analytically and numerically. Numerical and semi-analytical comparisons of electromagnetic torque and back EMF are shown in Figures 11 and 12.

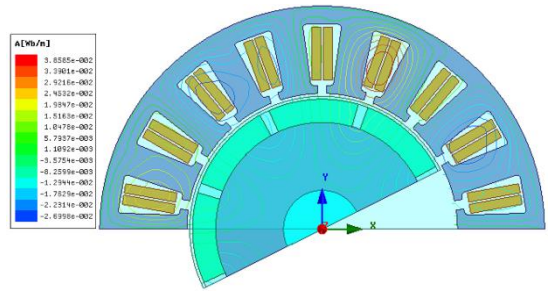

(a) Conventional Surface mounted

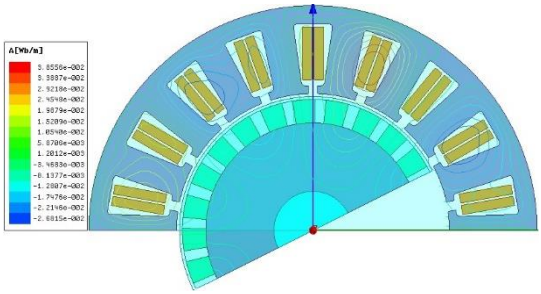

(b) SHPM-D1

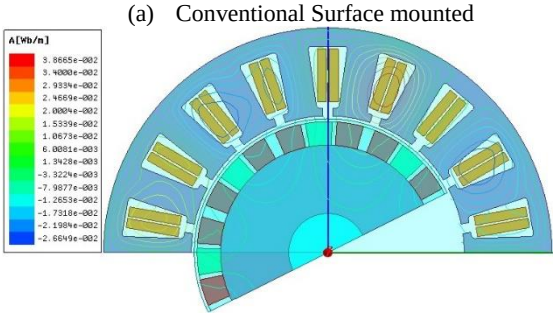

(c) SHPM-D2

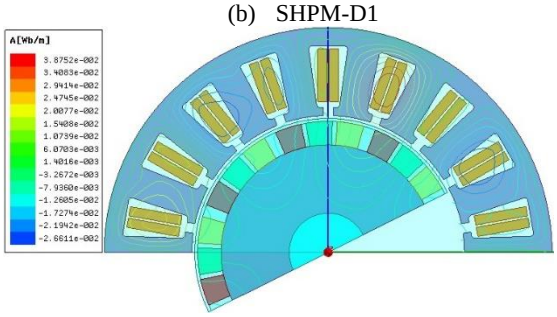

(d) SHPM-D3

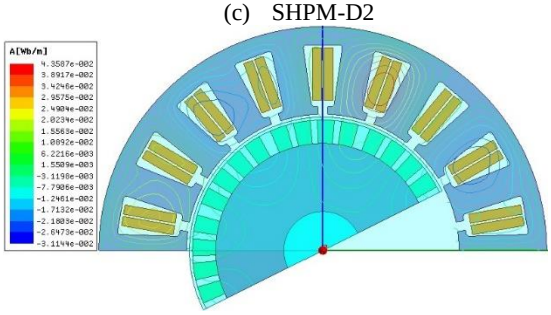

(e) SHPM-D4

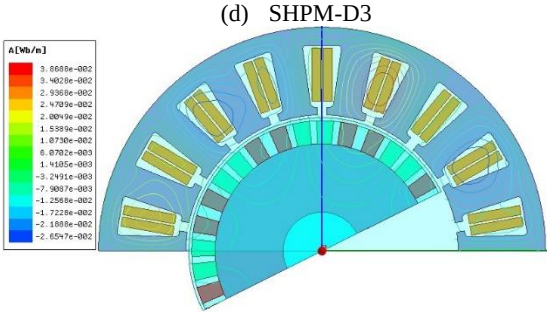

(f) SHPM-D5

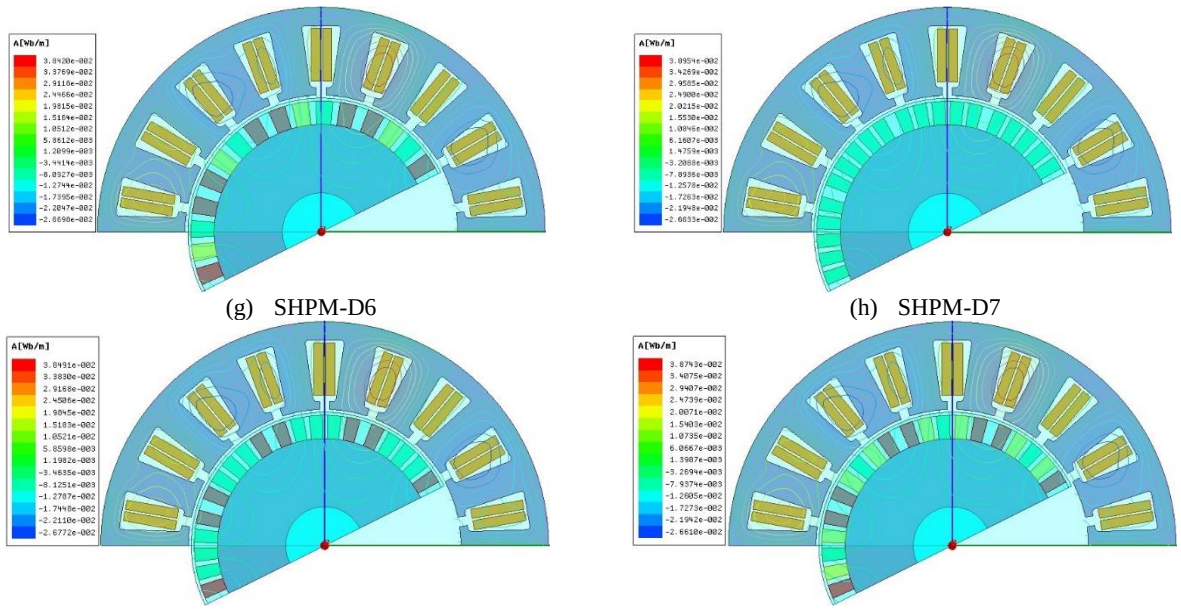

(g) SHPM-D6 (h) SHPM-D7

(i) SHPM-D8 (j) SHPM-D9

Fig. 6 Flux lines distribution in the investigated SHPM machines.

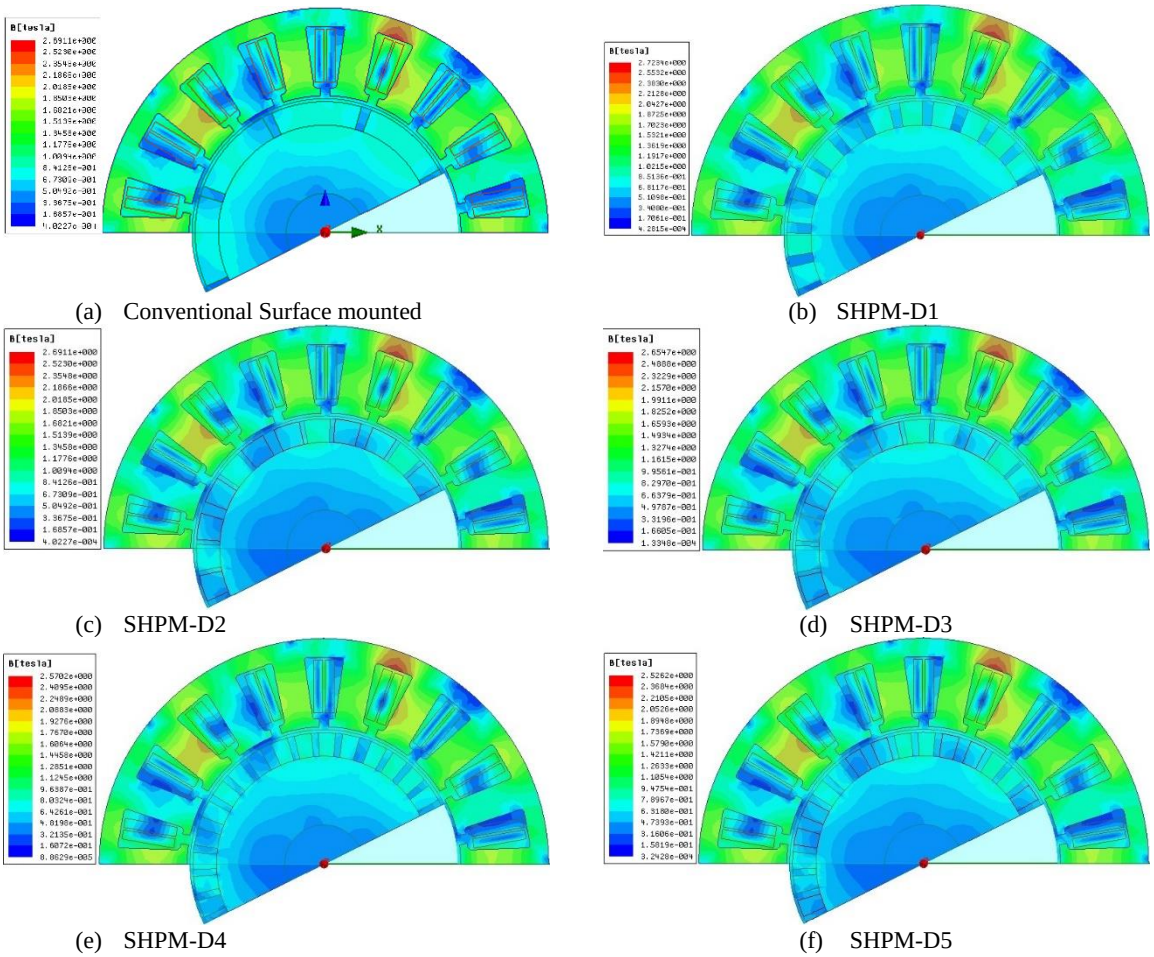

(a) Conventional Surface mounted (b) SHPM-D1

(c) SHPM-D2 (d) SHPM-D3

(e) SHPM-D4 (f) SHPM-D5

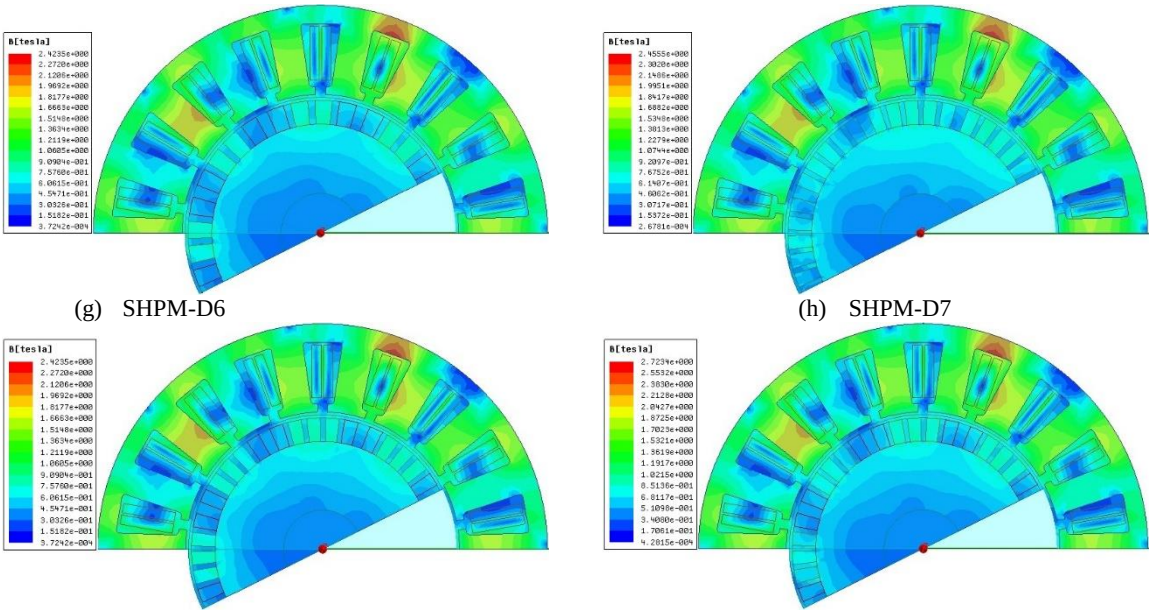

(g) SHPM-D6 (h) SHPM-D7

(i) SHPM-D8 (j) SHPM-D9

Fig. 7 Magnetic flux density distribution in the investigated SHPM machines.

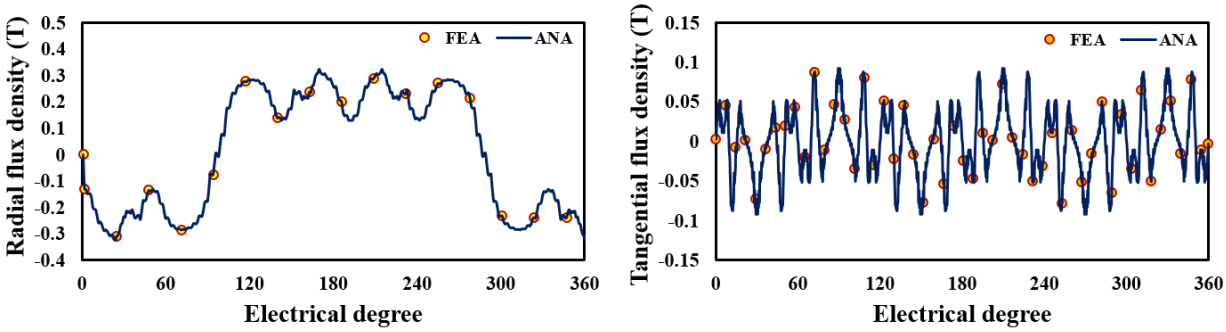

(a) Radial component (b) Tangential component

Fig. 8 A comparison of semi-analytical and numerical computation of the no-load air-gap field plot in main air-gap for similar SHPM machine type.

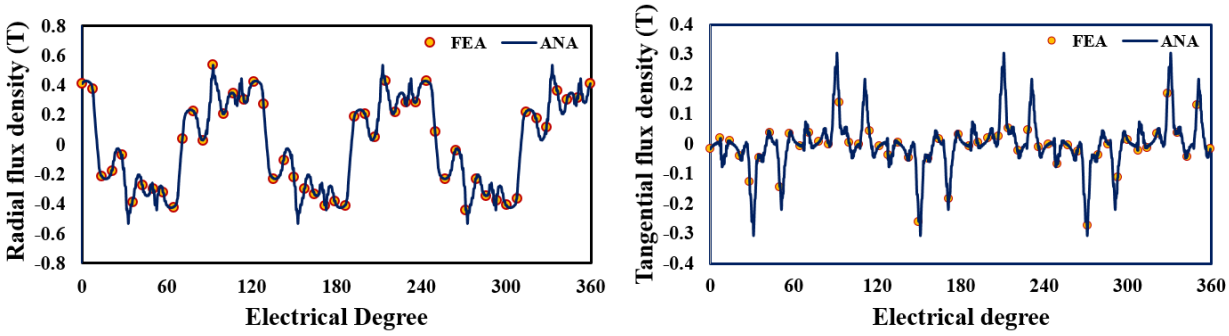

(a) Radial component (b) Tangential component

Fig. 9 A comparison of analytical and numerical computation of the on-load-1 air-gap field plot in main air-gap for similar SHPM machine type.

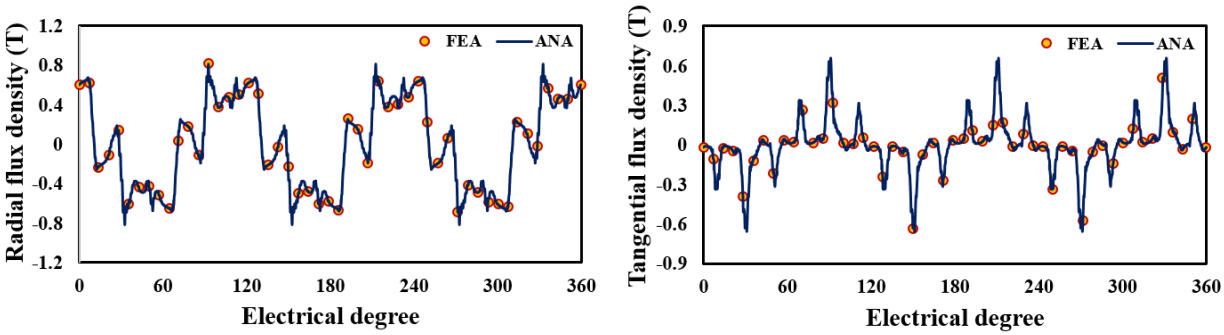

(a) Radial component (b) Tangential component

Fig. 10 A comparison of analytical and numerical computation of the on-load-2 air-gap field plot in main air-gap for similar SHPM machine type.

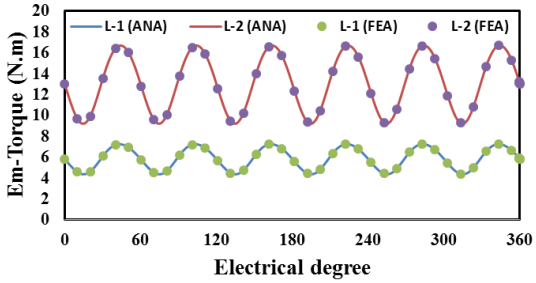

Fig. 11 A comparison of analytical and numerical computation of the on-load-2 electromagnetic torque for similar SHPM machine type.

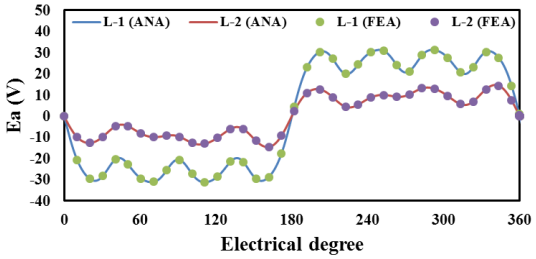

Fig. 12 A comparison of analytical and numerical computation of the on-load-2 electromagnetic torque for similar SHPM machine type.

3.3 Generation Operation Mode in Hybrid Electric Vehicle

In charging mode, the SHPM rotor and windings act as a generator. In this case, a lot of energy is stored in the battery. When the SHPM rotor rotates at 1500 rpm, the generator-induced voltage equals the voltage shown in Table 12, called charge mode.

Table 12 A comparison between induced voltages of the studied machines at charging mode.

Machine type	Induced voltage at rated speed, V
conventional	10.03
D1	8.67
D2	26.23
D3	59.25
D4	45.02
D5	25.95
D6	8.10
D7	36.10
D8	6.39
D9	24.55

3.4 Semi-Analytical and Experimental Comparison

This section first presents the fabrication steps for the various parts of the SHPM machine, then describes the experimental tests. Table 10 shows the materials and sizes of the machine parts investigated. The rotor core is made from M-19 steel laminations using a laser cutting process. NdFeB, Alnico, and SeCo PMs with residual flux densities of Br = 1.17T, 0.72T, and 0.86T, respectively, are used in the rotor core. MO-45 steel is used to manufacture machine shafts due to its high static/dynamic strength. The manufactured mechanical elements are shown in Figures 13, 14, and 15.

Table 13 Parts material and their dimensions.

Stator			SHPM Rotor		
Part Name	Material	Dimension	Part Name	Material	Dimension
Lamination	M-19	0.5mm	Lamination	M19	0.5mm
Caps	Al	5.5mm	PM	NdFeB	
Wire	Cu	1mm*20		Alnico	
				SeCo	
			Shaft	MO-45	L=100mm D=10mm
The effective length of the rotor: 20 mm					

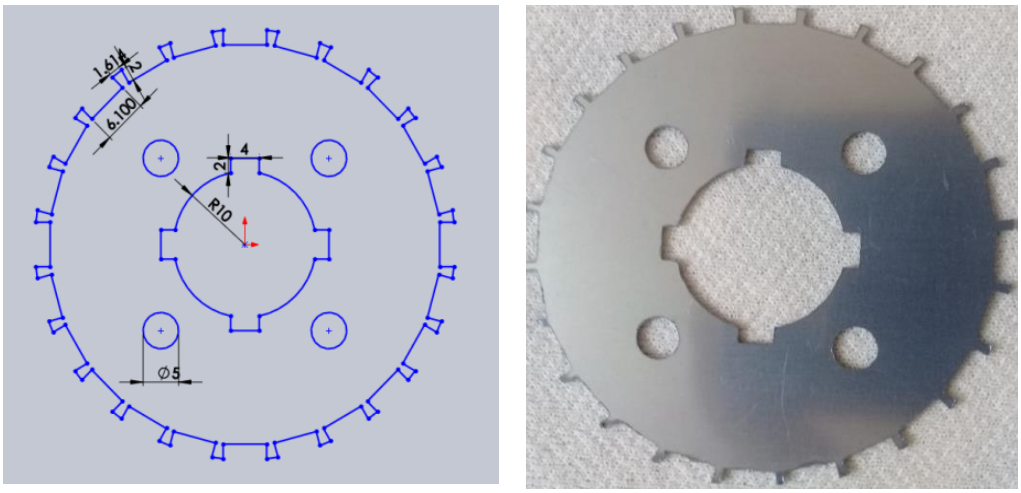

(a) (b)

Fig.13 (a) Cad model and (b) fabricated lamination of SHPM rotor

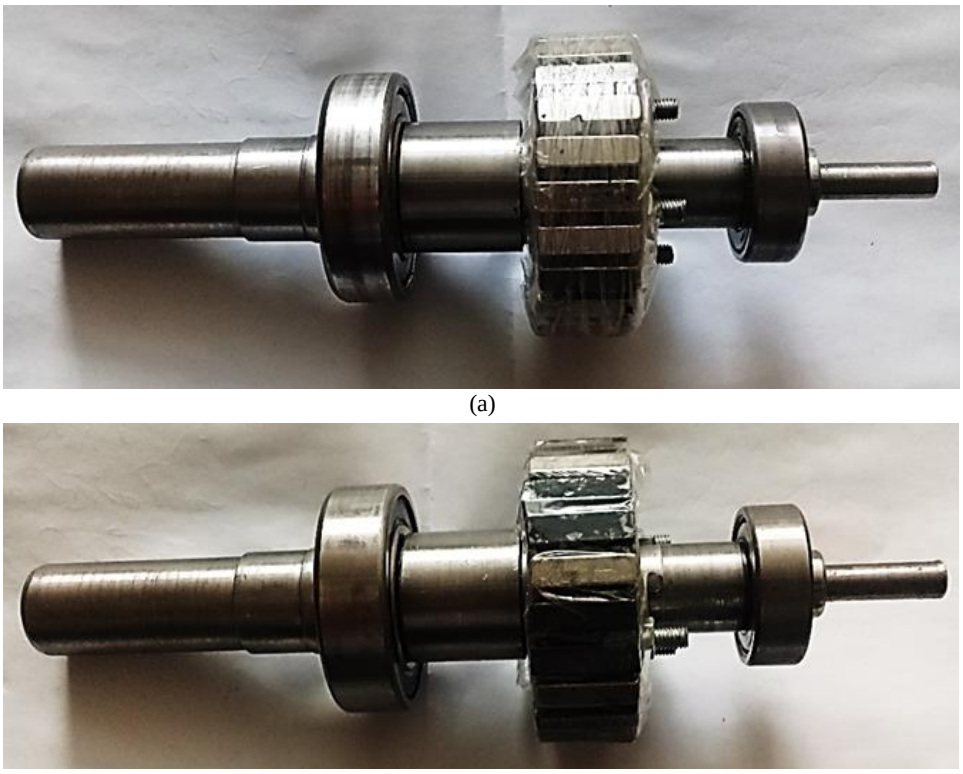

(a)

(b)

Fig. 14 The fabricated rotors. (a) similar material rotor, (b) dissimilar material rotor.

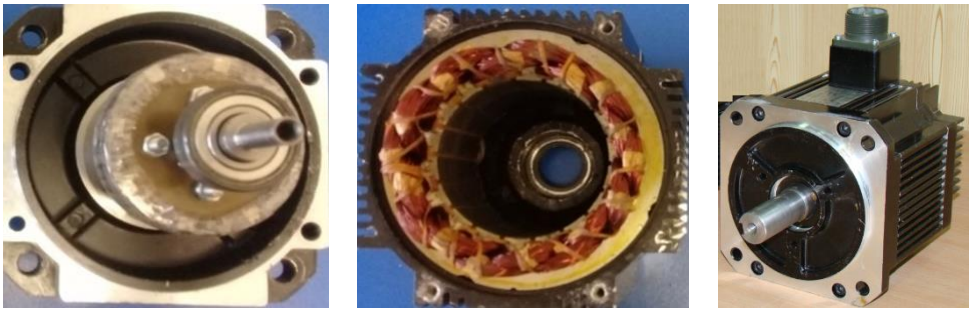

(a) (b) (c)

Fig. 15 The fabricated SHPM machine parts, (a) SHPM rotor, (b) stator, (c) assembled motor.

Figure 16 shows how the SHPM motor and generator are connected to the power supply and oscilloscope. Note that the 3 phases of the machine are connected in the star mode. To analyze the performance of the SHPM machine, the generator is connected to a PM DC motor rated at 1500 rpm and shaft is aligned. It also uses a light sensor to determine speed.

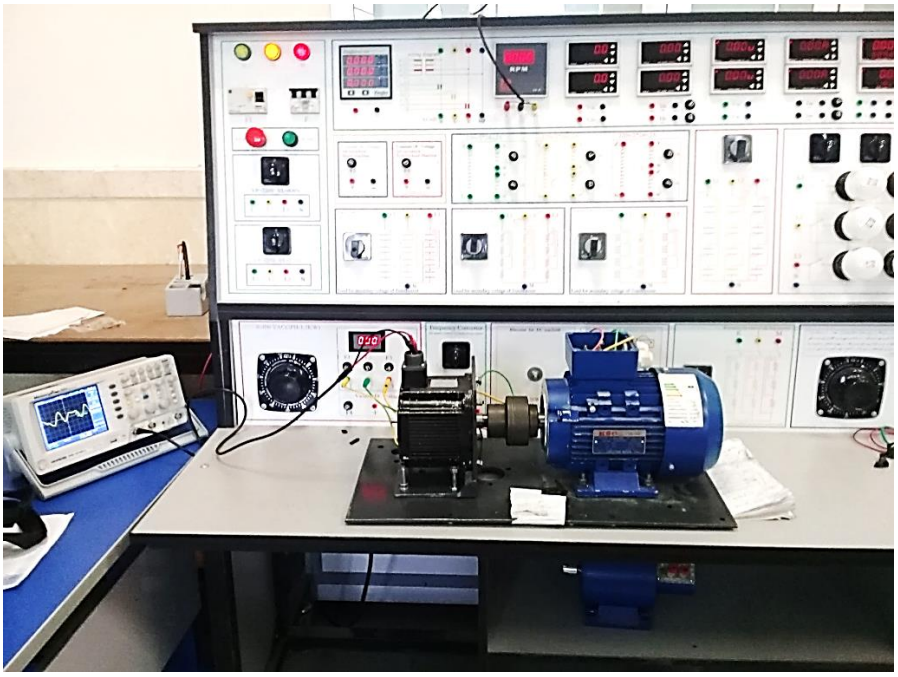

Fig. 16 The fabricated SHPM machine under experimental tests.

4 Conclusion

A new SHPM machine with nine topologies has been investigated semi-analytical, numerically, and experimentally. In this study, we compared the magnetic torque, torque ripple, and charging voltage of these topologies. The proposed machine has attractive features that can improve pulsating torque and reduce cost, noise, and vibration. A subdomain-based analytical model was presented to calculate the performance characteristics of SHPM machines. In this method, we divided the machine model into several different regions and examined the PDE expression in each region using the appropriate boundary conditions (BC) and interface conditions (IC). We applied this model to calculate the performance of the prototype SHPM machine, and the results of the proposed model were validated with an error percentage of about 3 thanks to the FEM and experimental test results.

Appendix

Table A1 Performance calculation of a 3-phase SHPM machine.

$T_e = \frac{L_s}{\mu_0}\int_0^{2\pi} BI_r(t_e.\theta)\cdot BI_\theta(t_e.\theta)d\theta$	$t_e = ln\left(\frac{R_2}{R_e}\right)$ $R_e = (R_2 + R_3)/2$	A(1)
$\begin{bmatrix}\psi_a\\ \psi_b\\ \psi_c\end{bmatrix} = N_c C^T[\varphi_1 \quad \varphi_2 \quad \varphi_3 \quad \dots \quad \varphi_{Q_2}]$		A(2)
$\varphi_i = -\frac{L_s {R_4}^2}{k_f S}\int_0^{\beta}\int_0^{t_8} A_{m_i}(t.\theta)\cdot e^{-2t}dtd\theta$		A(3)
$\begin{bmatrix}\psi_a\\ \psi_b\\ \psi_c\end{bmatrix} = \begin{bmatrix}\psi 1_a\\ \psi 1_b\\ \psi 1_c\end{bmatrix} + \begin{bmatrix}\psi 2_a\\ \psi 2_b\\ \psi 2_c\end{bmatrix}$	$\begin{bmatrix}\psi 1_a\\ \psi 1_b\\ \psi 1_c\end{bmatrix} = \frac{N_c}{2} C_1^T[\varphi_{11} \quad \varphi_{12} \quad \varphi_{13} \quad \dots \quad \varphi_{1Q_2}]$ $\begin{bmatrix}\psi 2_a\\ \psi 2_b\\ \psi 2_c\end{bmatrix} = \frac{N_c}{2} C_2^T[\varphi_{21} \quad \varphi_{22} \quad \varphi_{23} \quad \dots \quad \varphi_{2Q_2}]$	A(4)
$\varphi_{1i} = -\frac{2L_s {R_4}^2}{k_f S}\int_0^{\frac{\beta}{2}}\int_0^{t_8} A_{m_i}(t.\theta)\cdot e^{-2t}dtd\theta$		A(5)

$\varphi_{2i} = -\frac{2L_s {R_4}^2}{k_f S} \int_{\frac{\beta}{2}}^{\beta} \int_0^{t_8} A_{m_i}(t.\theta) \cdot e^{-2t} dt d\theta$		A(6)
$E_a = \omega \frac{d\psi_a}{d\theta_r}$		A(7)
$L_a = \frac{\psi_a}{I_A}$		A(8)
$M_{AB} = \frac{N\varphi_{AB}}{I_B}$		A(9)
$T_R = \frac{T_{max} - T_{min}}{T_{av}}$		A(10)

References

[1] Tahanian, Hamed, Mehdi Aliahmadi, and Jawad Faiz. "Ferrite permanent magnets in electrical machines: Opportunities and challenges of a non-rare-earth alternative." *IEEE Transactions on Magnetics* 56.3 (2020): 1-20.

[2] Jahns, Thomas. "Getting rare-earth magnets out of EV traction machines: A review of the many approaches being pursued to minimize or eliminate rare-earth magnets from future EV drivetrains." *IEEE Electrification Magazine* 5.1 (2017): 6-18.

[3] Rinderknecht, S., and T. Meier. "Electric power train configurations and their transmission systems." *SPEEDAM 2010*. IEEE, 2010.

[4] Wang, Weinan, et al. "Demagnetization and permanent-magnet minimization analyses of less-rare-earth interior permanent-magnet synchronous machines used for electric vehicles." *IEEE Transactions on Magnetics* 54.11 (2018): 1-5.

[5] Constantin, A. I., Dumitru, C., Tudor, E., Vasile, I., & Arsene, M. (2021, May). Studies Related to the Optimization of an Interior Permanent Magnet Synchronous Machine Designed for the Electric Vehicles. In *2021 International Conference on Applied and Theoretical Electricity (ICATE)* (pp. 1-5). IEEE.

[6] Wu, S., Tian, L., & Cui, S. (2008, September). A comparative study of the interior permanent magnet electrical machine's rotor configurations for a single shaft hybrid electric bus. In *2008 IEEE Vehicle Power and Propulsion Conference* (pp. 1-4). IEEE.

[7] Hamiti, T., Benlamine, R., Vangraefschepe, F., & Lhotellier, D. (2016, November). Selection of rare-earth-free permanent magnet machine for C-segment electric vehicle: Comparative analysis of different machine topologies. In *2016 International Conference on Electrical Systems for Aircraft, Railway, Ship Propulsion and Road Vehicles & International Transportation Electrification Conference (ESARS-ITEC)* (pp. 1-6). IEEE.

[8] Yu, C., Chau, K. T., & Jiang, J. Z. (2008, September). A permanent-magnet flux-mnemonic integrated-starter-generator for hybrid electric vehicles. In *2008 IEEE Vehicle Power and Propulsion Conference* (pp. 1-6). IEEE.

[9] Alamoudi, Y. A., Atkinson, G. J., Mecrow, B. C., & Zhang, M. (2012, October). A new high torque density permanent magnet machine design for electric vehicles. In *IECON 2012-38th Annual Conference on IEEE Industrial Electronics Society* (pp. 2348-2353). IEEE.)

[10] Hafner, M., Finken, T., Felden, M., & Hameyer, K. (2011). Automated virtual prototyping of permanent magnet synchronous machines for HEVs. *IEEE Transactions on Magnetics*, *47*(5), 1018-1021.

[11] Zhu, X., Yang, S., Du, Y., Xiang, Z., & Xu, L. (2016). Electromagnetic performance analysis and verification of a new flux-intensifying permanent magnet brushless motor with two-layer segmented permanent magnets. *IEEE Transactions on Magnetics*, *52*(7), 1-4.

[12] Guo, S., Guo, H., & Xu, J. (2018, October). Design and comparison of six-phase fault-tolerant interior permanent magnet motor and surface-mounted permanent magnet motor for electric vehicles. In *2018 21st International Conference on Electrical Machines and Systems (ICEMS)* (pp. 120-125). IEEE.

[13] M. Lukaniszyn, M. Jagiela, and R. Wrobel, "Optimization of permanent magnet shape for minimum cogging torque using a genetic algorithm," *IEEE Trans. on Magn.*, Vol. 40, No. 2, pp. 1228-1231, 2004.

[14] D. C. Hanselman, "Effect of skew, pole count and slot count on brushless motor radial force, cogging torque and back EMF," *IEE Proc. Electrical Power Application*, Vol. 144, No. 5, pp. 325-330, 1997.

[15] R. Lateb, N. Takorabet, and F. Meibody-Tabar, "Effect of magnet segmentation on the cogging torque in surface-mounted permanent-magnet motors," *IEEE Trans. on Magn.*, vol. 42, no. 3, pp. 442-445, 2006.

[16] B. Ackermann, J. H. H. Janssen, R. Sottek and R. I. van Steen, "New technique for reducing cogging torque in a class of brushless DC motors," *IEE Proc.-B*, Vol. 139, No. 4, pp. 315-320, 1992.

[17] T. Ishikawa, and G. R. Slemon, "A method of reducing ripple torque in permanent magnet motors without skewing," *IEEE Trans. on Magn*, Vol. 29, No. 2, pp.2028-2031, 1993.

[18] A. Keyhani, C. Studer, T. Sebastian, and S. K. Murth, "Study of cogging torque in permanent magnet motors," Electric Machines and Power Systems, vol. 27, no. 7, pp. 665-678, July 1999.

[19] T. Li, and G. Slemon, "Reduction of cogging torque in permanent magnet motors," *IEEE Trans. on Magn*., Vol. 24, No. 6, pp. 2901-2903, 1988.

[20] C. C. Hwang, S. B. John, and S. S. Wu, "Reduction of cogging torque in spindle motors," *IEEE Trans. on Magn.*, Vol. 34, No. 2, pp. 468-470, 1998.

[21] Jabbari, A. "The Effect of Dummy Slots on Machine Performance in Brushless Permanent Magnet Machines: An Analytical, Numerical, and Experimental Study." *Iranian Journal of Electrical and Electronic Engineering* (2022): 2284-2284.

[22] Jabbari, A. "Analytical modeling of magnetic field distribution in inner rotor brushless magnet segmented surface inset permanent magnet machines." *Iranian Journal of Electrical and Electronic Engineering* 14.3 (2018): 259-269.

[23] Z. Q. Zhu and D. Howe, "Instantaneous magnetic-field distribution in brushless permanent-magnet dc motor, part III: Effect of slotting," *IEEE Trans. Magn.*, Vol. 29, No. 1, pp. 143–151, Jan. 1993.

[24] M. Markovic, M. Jufer, and Y. Perriard, "Reducing the cogging torque in brushless dc motors by using conformal mappings," *IEEE Trans. Magn.*, Vol. 40, No. 2, pp. 451–455, Mar. 2004.

[25] D. Zarko, D. Ban, and T. A. Lipo, "Analytical calculation of magnetic field distribution in the slotted air gap of a surface permanent-magnet motor using complex relative air-gap permeance," *IEEE Trans. Magn.*, Vol. 42, No. 7, pp. 1828–1837, Jul. 2006.

[26] K. Boughrara, D. Zarko, R. Ibtiouen, O. Touhami, and A. Rezzoug, "Magnetic field analysis of inset and surface-mounted permanent- magnet synchronous motor using Schwarz-Christoffel transformation," *IEEE Trans. Magn.*, Vol. 45, No. 8, pp. 3166–3168, Aug.2009.

[27] Q. Gu and H. Gao, "Effect of slotting in PM electrical machines," *Elect. Mach. Power Syst.*, Vol. 10, pp. 273–284, 1985.

[28] N. Boules, "Prediction of no-load flux density distribution in permanent magnet machines," *IEEE Trans. Ind. Appl.*, Vol. IA-21, No. 3, pp. 633–643, Jul./Aug. 1985.

[29] B. Ackermann and R. Sottek, "Analytical modeling of the cogging torque in permanent magnet motors," *Elect. Eng.*, Vol. 78, No. 2, pp. 117–125, Mar. 1994.

[30] K. F. Rasmussen, H. D. John, T. J. E. Miller, M. I. McGilp, and O. Mircea, "Analytical and numerical computation of air-gap magnetic field in brushless motors with surface permanent magnet," *IEEE Trans. Magn.*, Vol. 36, No. 6, pp. 1547–1554, Nov./Dec. 2000.

[31] X. Wang, Q. Li, S. Wang, and Q. Li, "Analytical calculation of air-gap magnetic field distribution and instantaneous characteristics of brushless dc motors," *IEEE Trans. Energy. Convers.*, Vol. 18, No. 3, pp. 386–391, Sep. 2003.

[32] Z. J. Liu and J. T. Li, "Analytical solution of air-gap field in permanent magnet motors taking into account the effect of pole transition over slots," *IEEE Trans. Magn.*, Vol. 43, No. 10, pp. 3872–3882, Oct. 2007.

[33] Z. J. Liu, J. T. Li, and Q. Jiang, "An improved analytical solution for predicting magnetic forces in permanent magnet motors," *J. Appl. Phys.*, Vol. 103, No. 7, 2008.

[34] Z. J. Liu and J. T. Li, "Accurate prediction of magnetic field and magnetic forces in permanent magnet motor using an analytical solution," *IEEE Trans. Energy. Convers.*, Vol. 23, No. 3, pp. 717–726, Sep. 2008.

[35] P. Kumar and P. Bauer, "Improved analytical model of a permanent magnet brushless dc motor," *IEEE Trans. Magn.*, Vol. 44, No. 10, pp. 2299–2309, Oct. 2008.

[36] T. Lubin, S. Mezani, and A. Rezzoug"Exact analytical method for magnetic field computation in the air gap of cylindrical electrical machines considering slotting effects", *IEEE Trans. on Magnetics*, Vol. 46, No. 4, pp.1092-1099, 2010

[37] B. L. J. Gysen, E. Ilhan, K. J. Meessen, J. J. H. Paulides and E. A. Lomonova "Modeling of Flux Switching Permanent Magnet Machines with Fourier Analysis", *IEEE Trans. Magnetics.*, Vol. 46, No. 6, pp. 1499-1502, June 2010.

[38] K. Boughrara, R. Ibtiouen, and T. Lubin "Analytical prediction of magnetic field in parallel double excitation and spoke-type permanent-magnet machines accounting for tooth-tips and shape of polar pieces", *IEEE Trans. on Magnetics*, Vol. 48, No. 7, pp.2121-2137, 2012.

[39] K. Boughrara, T. Lubin, and R. Ibtiouen, "General subdomain model for predicting

magnetic field in internal and external rotor multiphase flux-switching machines topologies", *IEEE Trans. on Magnetics*, Vol. 49, No. 10, pp.5310-5325, 2013.
[40] T.L. Tiang, D. Ishak, and M.K.M. Jamil, "Complete subdomain model for surface-mounted permanent magnet machines", In *Energy Conversion (CENCON), 2014 IEEE Conference on*, pp. 140-145, October 2014.
[41] X. Liu, H. Hu, J. Zhao, A. Belahcen, L. Tang and L. Yang," Analytical Solution of the Magnetic Field and EMF Calculation in Ironless BLDC Motor. *IEEE Trans. on Magnetics*, Vol. 52, No. 2, pp.1-10, 2016.
[42] B. Dianati, H. Heydariand S.A. Afsari"Analytical Computation of Air-Gap Magnetic Field in a Viable Superconductive Magnetic Gear", *IEEE Trans. on Applied Superconductivity*, Vol. 26, No. 6, pp.1-12, 2016.
[43] A. Jabbari "An Analytical, Numerical and Experimental Study on Performance Characteristics in a Novel Vernier Permanent Magnet Machine", *Electrical Engineering*, Vol. 102, No. 4, pp. 2369-2379, 2020.
[44] Fu WN and Liu Y. A unified theory of flux-modulated electric machines. In: 2016 International symposium on electrical engineering (ISEE)14 December 2016, pp. 1– 13. New York: IEEE
[45] Rahideh A and Korakianitis T. Analytical magnetic field distribution of slotless brushless permanent magnet motors – Part I. Armature reaction field, inductance and rotor eddy current loss calculations. IET Electric Power Appl 2012; 6(9): 628–638.
[46] Rahideh A and Korakianitis T. Analytical magnetic field distribution of slotless brushless PM motors. Part 2: open-circuit field and torque calculations. IET Electric Power Appl 2012; 6(9): 639–651.
[47] Rahideh A, Mardaneh M and Korakianitis T. Analytical 2-D calculations of torque, inductance, and back-EMF for brushless slotless machines with surface inset magnets. IEEE Trans Magn 2013; 49(8): 4873–4884.
[48] Rahideh A and Korakianitis T. Analytical magnetic field calculation of slotted brushless permanent-magnet machines with surface inset magnets. IEEE Trans Magn 2012; 48(10): 2633–2649.
[49] Teymoori S, Rahideh A, Moayed-Jahromi H, et al. 2-D analytical magnetic field prediction for consequent-pole permanent magnet synchronous machines. IEEE Trans Magn 2016; 52(6): 1–14.
[50] Moayed-Jahromi H, Rahideh A and Mardaneh M. 2-D analytical model for external rotor brushless PM machines. IEEE Trans Energy Convers 2016; 31(3): 1100– 1109.
[51] Jabbari A. Analytical modeling of magnetic field distribution in inner rotor brushless magnet segmented surface inset permanent magnet machines. J Electr Eng 2018; 69(1): 39–45.
[52] Jabbari A. An analytical expression for magnet shape optimization in surface-mounted permanent magnet machines. Math Comput Appl 2018; 23(4): 57.
[53] Shen Y and Zhu Z. General analytical model for calculating electromagnetic performance of permanent magnet brushless machines having segmented Halbach array. IET Electr Syst Transp 2013; 3(3): 57–66.
[54] Jabbari A. analytical modeling of magnetic vector potential in surface inset permanent magnet machines. Iran J Electr Electron Eng 73.
[55] Jabbari A and Dubas F. A new subdomain method for performances computation in interior permanent-magnet (IPM) machines. Iran J Electr Electron Eng 2020; 16(1): 26–38.
[56] Jabbari A. Exact analytical modeling of magnetic vector potential in surface inset permanent magnet DC machines considering magnet segmentation. J Electr Eng 2020; 69(1): 39–45.
[57] Jabbari A. Analytical modeling of magnetic field distribution in multiphase H-type stator core permanent magnet flux switching machines. Iran J Sci Technol Trans Electr Eng 2019; 43:389–401.
[58] Jabbari A. An analytical study on iron pole shape optimization in high-speed interior permanent magnet machines. Iran J Sci Technol Trans Electr Eng 2020; 44(1): 169–174.
[59] Jabbari A, Taheri H and Ghadimi AA. An analytical, numerical and experimental study on performance characteristics in a novel Vernier Permanent Magnet Machine. Elect Eng 2020; 102(4): 2369–2379.
[60] Wu YC and Jian BS. Magnetic field analysis of a coaxial magnetic gear mechanism by two-dimensional equivalent magnetic circuit network method and finite-element method. Appl Math Model 2015; 39(19): 5746–5758.

Ali Jabbari was born in Shazand, Iran, in 1980. He received the B.Sc. degree from the "Iran University of Science and Technology" in 2002 and his M.Sc. and PhD degrees both in Mechanical Engineering from "Mazandran University" in 2004 and 2009, respectively, with a focus on the design and the optimization

of Brushless DC permanent magnet machines for direct drive applications. He is currently an Associate Professor with the Department of Mechanical Engineering, Arak University, Arak, Iran. Since 2014, he has been the Head of "Gearless Wind Turbine Project" team. **Interests:** Gearless Wind Turbine Design, Analytical Modeling, PM Machines, Subdomain Technique, Friction Stir Welding, Metal Forming.

Ali Badran was born in Arak, Iran, in 1975. He received the B.Sc. degree in agricultural engineering with a focus on agricultural machine mechanics in 2017 and his M.Sc. degree in mechanical engineering with a focus on construction and production in 2019 with a focus on the design and optimization of permanent magnet synchronous generators for use in Wind turbines from Arak University. He is currently an art student in the field of construction and production at Shahid Moghimi Academy of Art, Arak, Iran. His research interests are in the field of designing systems and machinery for manufacturing products, oil and gas and petrochemical valves, metal molds, electric machines, etc.